MODELLING BEHAVIOUR OF HIGH-STRENGTH CONCRETE BEAMS

Piotr Smarzewski

Pope John Paul II State School of Higher Education in Biała Podlaska,
Faculty of Economic and Technical Sciences, Department of Technical Sciences,
Sidorska Street 95/97, 21-500 Biała Podlaska, Poland
e-mail: p.smarzewski@pollub.pl

Summary:
The comparative analysis of the own numerical results with experimental results was presented for the examples of the reinforced high-strength concrete beams under static load. The arc-length method was used in combination with Newton-Raphson method to trace the complete response in load-deformation space. The comparison of the obtained results indicates on the correctness of the assumptions and constitutive models of the high-strength concrete and reinforcement steel, and the effectiveness of the solution method. Numerical results of smeared crack patterns are qualitatively agreeable, for the localization, the direction and the concentration with experimental results. The development of strain in outer concrete layer of the compression zone and the development of strain for longitudinal reinforcement have excellent agreement in the most presented cases. The full nonlinear load-deformation at midspan response of the model produced compares well with the experimental response taken from literature. In the presented paper the usefulness of the arc-length method was verified on a spatial numerical model of the reinforced concrete beams with consideration of the concrete softening during compression and tension. The numerical solutions obtained for the reinforced concrete beams are coherent with the experimentally obtained results.

Keywords: Finite Element Method, beams, reinforced high-strength concrete.

Introduction

Improved performance computing systems and the possibility of their use in the design of engineering structures enforces intensive development of numerical methods for the calculation of static and dynamic analysis of structural behavior. Numerical methods are the only way to achieve practically useful solutions to complex spatial members with materials not subjected to the laws of linear elasticity.

A high performance concrete, the concrete of high strength and also high tightness, includes all the components previously applied to the concrete, but in different proportions dosed. Detailed information regarding the classification and characteristics of the composite cement-based materials have been presented in the works (Aïtcin 1998, Calderon 2009).

The subject of work is the reinforced high-strength concrete beams considered as composition of materials consisting of reinforced concrete steel rods distributed discretely in the concrete matrix. The purpose of the work is modelling the mechanisms of destruction of reinforced concrete beams loaded statically, the static deformation processes reinforced high-strength concrete beams, taking into account the physical nonlinearity of structural materials.

Modelling of concrete

The equations of the limit surfaces for concrete are described in the papers of (Willam, Warnke 1975, Ottosen 1977, Klisiński 1984, Stolarski 2004). The proposed equations depend on the limit surfaces of the first invariant of the stress tensor and the second and third invariant of the stress deviator. Such a description allows the most faithful approximation of concrete experimental results in complex stress states. In this paper, limit surface equation depending on five stress invariants in accordance with the theory of (Willam, Warnke 1975) and its proposal of the surface evolution law as a function of strain.

The failure criterion of concrete in a complex state of stress is described in the following expression:

$$F / f_c - S \geq 0, \tag{1}$$

in which: F - the function of stresses conditions $\sigma_{xp}, \sigma_{yp}, \sigma_{zp}$ in the direction of the Cartesian coordinate system x, y, z, S - failure surface dependant on the principal stresses $\sigma_1, \sigma_2, \sigma_3$, where: $\sigma_1 = \max\left(\sigma_{xp}, \sigma_{yp}, \sigma_{zp}\right)$, $\sigma_3 = \min\left(\sigma_{xp}, \sigma_{yp}, \sigma_{zp}\right)$ and $\sigma_1 \geq \sigma_2 \geq \sigma_3$ and five strength parameters: f_c - uniaxial compressive strength causing crashing, f_t - uniaxial tension strength causing cracking, f_{cb} - ultimate biaxial compressive strength causing crashing, f_1 - ultimate compressive strength for a state of biaxial compression superimposed on hydrostatic stress state σ_h^a and f_2 - ultimate compressive strength for a state of uniaxial compression superimposed on hydrostatic stress state σ_h^a.

The description failure of concrete is defined in four domains of stresses: compression – compression – compression, when $0 \geq \sigma_1 \geq \sigma_2 \geq \sigma_3$, tension – compression – compression, as $\sigma_1 \geq 0 \geq \sigma_2 \geq \sigma_3$, tension – tension – compression, when $\sigma_1 \geq \sigma_2 \geq 0 \geq \sigma_3$ and tension – tension – tension, as $\sigma_1 \geq \sigma_2 \geq \sigma_3 \geq 0$.

In each range of strain, independent functions F_1, F_2, F_3, F_4 and S_1, S_2, S_3, S_4 describe the function state of stresses F and the failure surface S. These functions in each of the state of stress are presented by (Smarzewski 2011).

Concrete limit surface with evolution laws is used as a criterion of destruction according to the following interpretation. The material is destroyed if the Eq. (1) is fulfilled. The state of failure can be distinguished as the state of cracking, if any principal stress is tensile, or the state of crushing, if all principal stresses are compressive. Safe working conditions describe the stress state interpreted as the elastic state inside the surface. Evolution of the limit surface is determined by the fallowing proposition of hardening or softening laws.

The essence of this proposition is shown in Figure 1. The stress-strain function for the uniaxial compressive phase of elastic-plastic strengthening and softening is confirmed in the experimental observations, indicating much larger the limit strains in the structural member than in the control plain concrete samples.

Interpreting the numerical results of the high-strength reinforced concrete beams, it was observed that the use of the equations describing relationships between strains and stresses proposed in (Model Code 90 1995) leads to a significant decrease in structural deflection. On the basis of numerical experiments in comparison with experimental results (Kamińska 1999, 2002) the concept of the behavior of high-strength concrete with uniaxial compression and tension in reinforced concrete was included in proposed model of concrete behaviour.

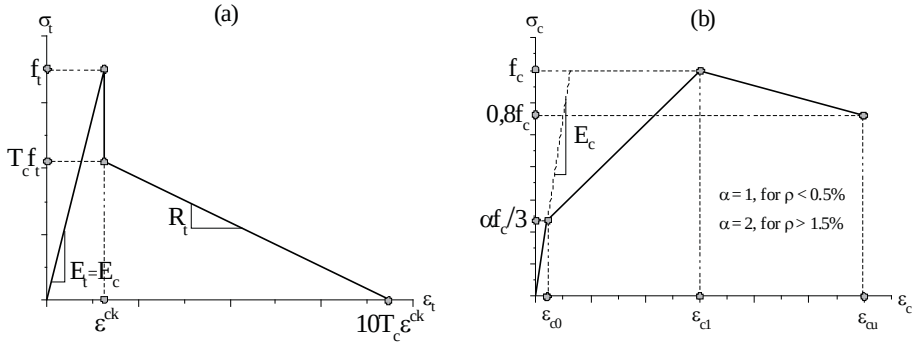

Figure 1. Assumed stress-strain relationship for concrete for uniaxial tension (a) and compression (b)

Stress-strain curve for tensile concrete (Fig. 2a) is linear up to the tensile strength f_t. It is assumed that the tensile deformation modulus is equal to the compressive one. After reaching f_t the cracks begin to develop. The brittle fracturing suddenly decrease the stress to a value greater or equal than $T_c f_t$. Value of parameter T_c should be chosen from the range $0.6 \le T_c \le 1$. The stiffening effect, included by founding a gradual, soft decrease of tensile strength to zero is described by strains equal to 0.8 ‰ if T_c = 0.6 and to 1.4 ‰ if T_c = 1.

The limit of elastic phase in the compressive concrete in relation to the reinforcement ratio was determined (Fig. 2b). For a reinforcement ratio greater than 1.5 % it was assumed linear stress-strain diagram to the level of 0.7 f_c, . Then begins the phase of elastic-plastic strengthening with linear increase in stress up to the uniaxial compressive strength f_c, and after then the stresses in concrete are decrease to 0.80 f_c at the limit strain ε_{cu}. For the proposed model strain ε_{c1} = 6 ‰ at the uniaxial compressive strength f_c and the limit compression strains ε_{cu} = 12 ‰ were assumed.

More slanted $\sigma - \varepsilon$ curve for the high-strength concrete is not always reflected in the behaviour of reinforced concrete elements. Experimental results (Lambrotte et al. 1990, Taerwe 1991, Bernardi 1999, Kamińska 1999) showed that low ductility concerns high-strength concrete in the structural elements is not justified. In such members, which were damaged by the crushing of concrete compression zone, the strains of concrete reached up to 6-12 ‰, and were appropriately twice the damaging strains registered on the plain concrete samples.

In the numerical analysis the hexahedral elements were applied for the concrete. Finite element is defined by the isotropic properties of the material, and eight nodes with three degrees of freedom in each of them, as the displacements of nodes in three-dimensional orthogonal local coordinate system. In each finite element at all points of the numerical integration the strains and stresses are calculate. Smeared crack model provides a description of the cracking at any point numerical integration in three directions perpendicular to the principal stresses. Crack formation is described by proposed model of concrete. In the graphical representation the results are presented in cracking outline form of a circle shape in the direction perpendicular to the principal stress. In the state of cracking or crushing concrete for the numerical balance in the finite element is added a small value of stiffness.

The matrix of elasticity for an isotropic material $\mathbf{D_c}$ is represented in the form:

$$\mathbf{D_c} = \frac{E_c}{(1+\nu_c)(1-2\nu_c)} \begin{bmatrix} 1-\nu_c & \nu_c & \nu_c & 0 & 0 & 0 \\ \nu_c & 1-\nu_c & \nu_c & 0 & 0 & 0 \\ \nu_c & \nu_c & 1-\nu_c & 0 & 0 & 0 \\ 0 & 0 & 0 & 0,5-\nu_c & 0 & 0 \\ 0 & 0 & 0 & 0 & 0,5-\nu_c & 0 \\ 0 & 0 & 0 & 0 & 0 & 0,5-\nu_c \end{bmatrix} \tag{2}$$

where: E_c - modulus of elasticity of concrete, ν_c - Poisson's ratio.

In the state of cracking and crushing the matrix is adapted to the state of the damage. In numerical modeling, it is necessary to take account of the characteristics of concrete description after they have formed. The parameter β_t is introduced as a multiplier for reducing shear transfer causing slip in the plane perpendicular to the cracks surface. The relationship between stress and strain of the cracked material in one plane is written in the form of a matrix:

$$\mathbf{D_c^{ck}} = \frac{E_c}{1+\nu_c} \begin{bmatrix} R_t(1+\nu_c)/E_c & 0 & 0 & 0 & 0 & 0 \\ 0 & 1/(1-\nu_c) & \nu_c/(1-\nu_c) & 0 & 0 & 0 \\ 0 & \nu_c/(1-\nu_c) & 1/(1-\nu_c) & 0 & 0 & 0 \\ 0 & 0 & 0 & 0,5\beta_t & 0 & 0 \\ 0 & 0 & 0 & 0 & 0,5 & 0 \\ 0 & 0 & 0 & 0 & 0 & 0,5\beta_t \end{bmatrix} \tag{3}$$

Graphical interpretation of the module weakness R_t and the multiplier for amount of tensile stress relaxation T_c is shown in Figure 2a. When cracks closing in the matrix $\mathbf{D_c^{ck}}$, shear parameter β_c is introduced:

$$\mathbf{D_c^{ck}} = \frac{E_c}{(1+\nu_c)(1-2\nu_c)} \begin{bmatrix} 1-\nu_c & \nu_c & \nu_c & 0 & 0 & 0 \\ \nu_c & 1-\nu_c & \nu_c & 0 & 0 & 0 \\ \nu_c & \nu_c & 1-\nu_c & 0 & 0 & 0 \\ 0 & 0 & 0 & \beta_c(0,5-\nu_c) & 0 & 0 \\ 0 & 0 & 0 & 0 & 0,5-\nu_c & 0 \\ 0 & 0 & 0 & 0 & 0 & \beta_c(0,5-\nu_c) \end{bmatrix} \tag{4}$$

Stiffness matrix for concrete cracked in two and three dimensions is written in the form:

$$\mathbf{D}_{\mathbf{c}}^{\mathbf{ck}} = E_c \begin{bmatrix} R_t / E_c & 0 & 0 & 0 & 0 & 0 \\ 0 & R_t / E_c & 0 & 0 & 0 & 0 \\ 0 & 0 & 1 & 0 & 0 & 0 \\ 0 & 0 & 0 & 0,5\beta_t / (1+\nu_c) & 0 & 0 \\ 0 & 0 & 0 & 0 & 0,5\beta_t / (1+\nu_c) & 0 \\ 0 & 0 & 0 & 0 & 0 & 0,5\beta_t / (1+\nu_c) \end{bmatrix} \tag{5}$$

and if the cracks are closed in two or three planes, the relationship is expressed in a matrix form Eq. (4). Opening or closing of cracks at the point of numerical integration depends on the sign of the cracking strains.

Modelling of steel

The simplified uniaxial model of steel for the reinforcing bars is used. The elastic-plastic material model with linear hardening, of identical stress-strain characteristics for the tension and compression. Spatial spar element, with two nodes with three degrees of freedom, was applied in the modeling of steel bars. Moreover, linear elastic model was assumed for the steel plates located in support and concentrated external force areas. To modeling of steel plates the hexahedral elements were applied.

Modelling of high-strength concrete beams

Spatial mesh steel rebar finite element was associated with the mesh of the concrete finite element by modeling the compatibility of displacements at common nodes. For such a mesh system the stiffness matrix is the sum of the finite element stiffness matrices for concrete and for reinforcement steel. In support areas steel plates were modeled as nodal imparting forces on steel rollers allow free rotation of the beam in the plane of bending. External concentrated force is also applied through the steel plate. Uniform distribution of forces at the nodes in the direction of the transverse symmetry axis of the steel plate was assumed.

The numerical model of spatial beams used dimensions and properties of the material as rectangular beams BP-1b and BP-2b investigated by (Kamińska 1999). Dimensions of beams with reinforcement and loading arrangements are shown in Fig. 2.

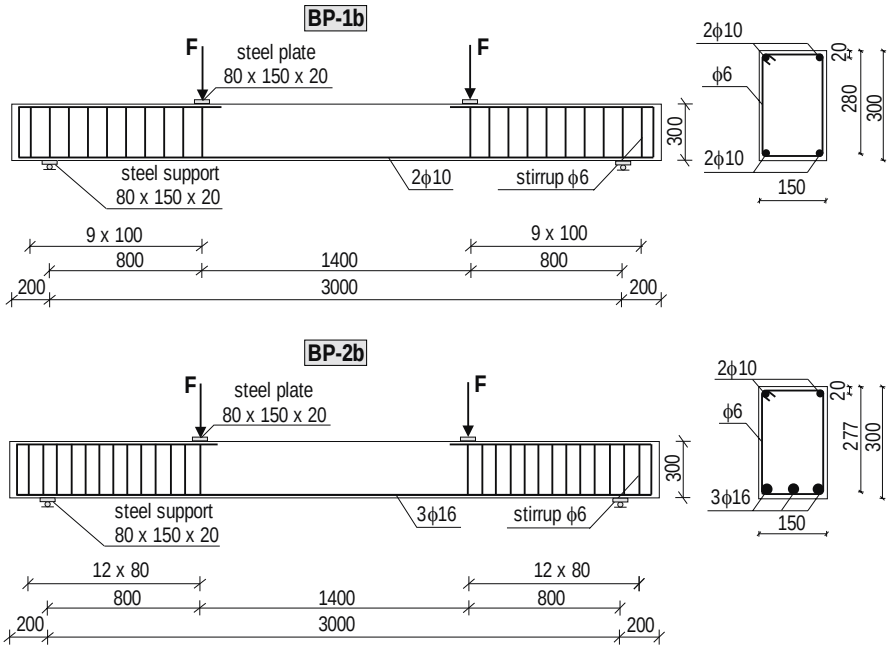

Fig. 2. Dimensions and cross-section of BP beams with reinforcement and loading arrangements

The parameters of constitutive concrete model are given for the beams BP-1b / BP-2b, respectively. High-strength concrete is defined by the uniaxial compressive strength f_c= 72.8 / 73.3 MPa, modulus of elasticity E_c= 34 / 35.8 GPa, tensile uniaxial strength f_t= 4.73 / 5.06 MPa, Poisson's ratio ν_c= 0.15, density ρ_c= 2600 kg/m^3, compressive strain at the strength stress level ε_{c1}= 6 ‰, ultimate compressive strain ε_{cu}= 12 ‰, shear transfer coefficients for an open crack β_t= 0.5 and shear transfer coefficients for the closed crack β_c= 0.99.

The appropriate material parameters for the steel bars of ϕ16/ϕ10/ϕ6 mm diameters are as follows: modulus of elasticity E_s= 196 / 194 / 201 GPa, yield stress f_y = 437 / 420 / 353 MPa, tensile uniaxial strength f_{st} = 713 / 624 / 466 MPa, limit strain at the yield stress ε_{su}= 106 / 116 / 75 ‰, modulus of plastic deformation E_T = 2659.7 / 1792.1 / 1542.8 MPa, Poisson's ratio ν_s= 0.3 and density ρ_s = 7800 kg/m^3.

Supporting and load transferring steel plate are defined by modulus of elasticity E_s = 210 GPa, Poisson's ratio ν_s= 0.3 and density ρ_s= 7800 kg/m^3. Having regard the longitudinal symmetry elements one half of the beams was modeled.

Methods of numerical solutions of the equilibrium equations

Newton-Raphson method with adaptive descent

Newton-Raphson method, shown graphically in Figure 3, is an iterative process of solving nonlinear equations

$$\mathbf{K}_i^T \Delta \mathbf{u}_i = \mathbf{F}^a - \mathbf{F}_i^{nr}, \tag{6}$$

$$\mathbf{u}_{i+1} = \mathbf{u}_i + \Delta \mathbf{u}_i, \tag{7}$$

where: $\mathbf{K}_i^T$ - tangent stiffness matrix, i - index corresponding to the number of the incremental step, $\mathbf{F}^a$ - generalized load vector, $\mathbf{F}_i^{nr}$ - vector of restoring loads representing the element internal loads in the discretised system.

Matrix $\mathbf{K}_i^T$ and vector $\mathbf{F}_i^{nr}$ are calculated on the basis of the displacement vector $\mathbf{u}_i$.

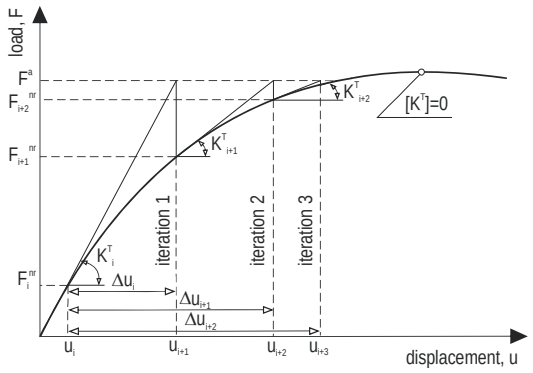

Fig. 3. Newton-Raphson method

Adaptive descent method presented in the work by (Eggert et al. 1991) is based on the change of solution path approximating the limit point and reversing along the secant until obtaining the convergence of numerical solution.

The stiffness matrix in Newton-Raphson equation Eq. (6) is described as a sum of two matrixes:

$$\mathbf{K}_i^T = \xi \mathbf{K}^S + (1-\xi)\mathbf{K}^T, \tag{8}$$

$\mathbf{K}^S$ - secant stiffness matrix, $\mathbf{K}^T$ - tangent stiffness matrix, ξ - adaptive descent parameter.

The method is based on the agreement adaptive descent parameter ξ in equilibrium iteration. The secant stiffness matrix is generated in the numerical method as a result of solving nonlinear tasks concerning material plastification, construction stiffness with large deformations or concrete crushing.

Arc-length method

In the method of numerical Crisfield's arc-length (Crisfield 1983), presented in Fig. 3 equation Eq. (6) is dependent on load parameter λ :

$$\mathbf{K}_i^T \Delta \mathbf{u}_i = \lambda \mathbf{F}^a - \mathbf{F}_i^{nr} . \tag{9}$$

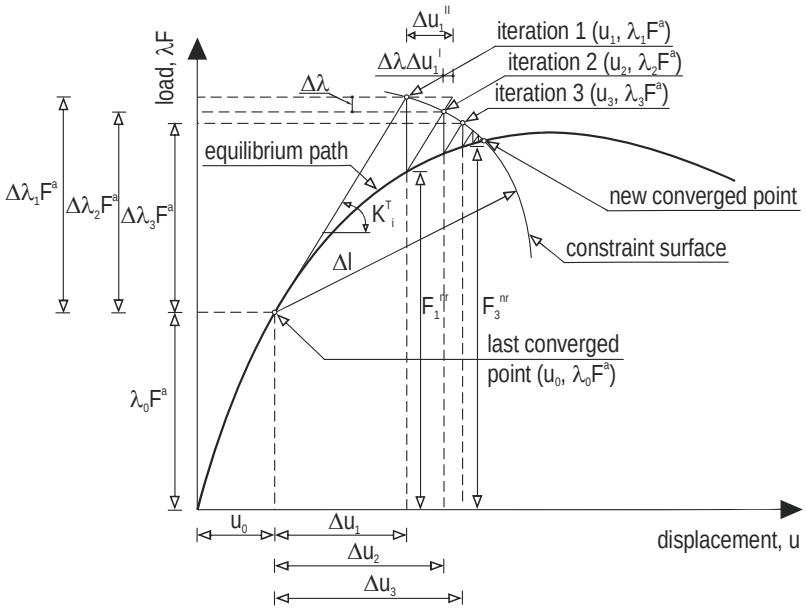

Fig. 3. Crisfield's arc-length method

In this procedure the variable load parameter λ is searched in the range $-1 \le \lambda \le 1$. In the incremental substep the equation has the following form:

$$\mathbf{K}_i^T \Delta \mathbf{u}_i - \Delta\lambda \mathbf{F}^a = \left(\lambda_0 + \Delta\lambda_i\right)\mathbf{F}^a - \mathbf{F}_i^{nr} , \tag{10}$$

$\Delta\lambda$ - incremental load parameter.

On the basis of equation Eq. (10) the vector of incremental displacement $\ddot{A}\mathbf{u}_i$ consists of two components described as follows

$$\Delta \mathbf{u}_i = \Delta\lambda \Delta \mathbf{u}_i^I + \Delta \mathbf{u}_i^{II}, \tag{11}$$

$\ddot{A}\mathbf{u}_i^I$ - vector of displacement increment caused by a unit load parameter, $\ddot{A}\mathbf{u}_i^{II}$ - vector of displacement increment in the Newton-Raphson method.

Displacement vectors are defined as

$$\Delta \mathbf{u}_i^I = \mathbf{K}_i^{T^{-1}} \mathbf{F}^a, \tag{12}$$

$$\Delta \mathbf{u}_{ii}^{II} = \mathbf{K}^{T^{-1}} \left[\left(\lambda_0 + \Delta\lambda_i \right) \mathbf{F}^{a} - \mathbf{F}^{nr} \right], \tag{13}$$

The incremental load parameter $\Delta\lambda$ is defined from the arc length equation:

$$l_i^2 = \Delta\lambda_i^2 + \beta^2 \Delta \mathbf{u}_n^{\ T} \Delta \mathbf{u}_n, \tag{14}$$

β - scaling factor, n - current step number, $\Delta \mathbf{u}_n$ - the sum of all displacement increments $\Delta \mathbf{u}_i$ in the current iteration step.

The work (Forde, Stiemer 1987) presents a general procedure of calculating the parameter $\Delta\lambda$ based on ensure orthogonality:

$$\Delta\lambda = \frac{r_i - \Delta \mathbf{u}_n^T \Delta \mathbf{u}_i^{II}}{\beta^2 \Delta\lambda_i + \Delta \mathbf{u}_n^T \Delta \mathbf{u}_i^{I}}, \tag{15}$$

r_i - unbalanced parameter obtained by scalar multiplication of normal and tangential vector.

The finale vectors are updated according to:

$$\Delta \mathbf{u}_{i+1} = \Delta \mathbf{u}_0 + \Delta \mathbf{u}_n + \Delta \mathbf{u}_i, \tag{16}$$

$$\lambda_{n+1} = \lambda_0 + \Delta\lambda_i + \Delta\lambda, \tag{17}$$

Iterations stop at the moment of obtaining the desired convergence of the numerical solution.

Numerical analysis high-strength concrete beams

Cracking analysis

The images of real cracks in full BP beams are presented against numerical images of smeared cracks for the left half of the beams with the same values of load in Figure 4.

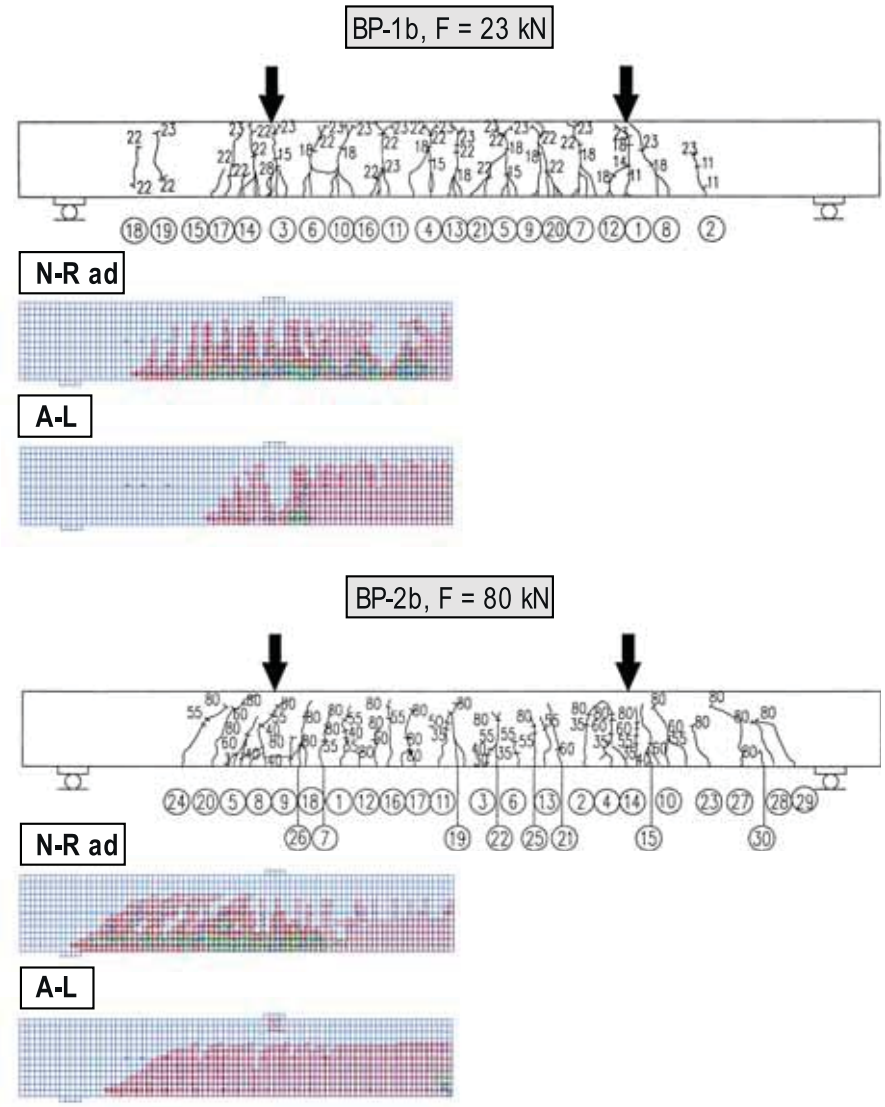

Fig. 4. Experimental and numerical images of cracking BP beams

All the obtained numerical results are in qualitative agreement with experimental results in terms of their location, direction and concentration. In case of Newton-Raphson method with adaptive descent slightly larger zone of smeared cracks was observed. Due to the lack stirrups in the model and experimental BP-1b beams with low reinforcement and BP-2b with a higher degree of reinforcement in the section of pure bending, arrangement of cracks is arbitrary.

Strain analysis

For the observation of strain changes in concrete, depending on the load, is assumed at the upper edge the point of the mid span of beams BP. The development of strain in the outer layer of the concrete compression zone are shown in Figure 5.

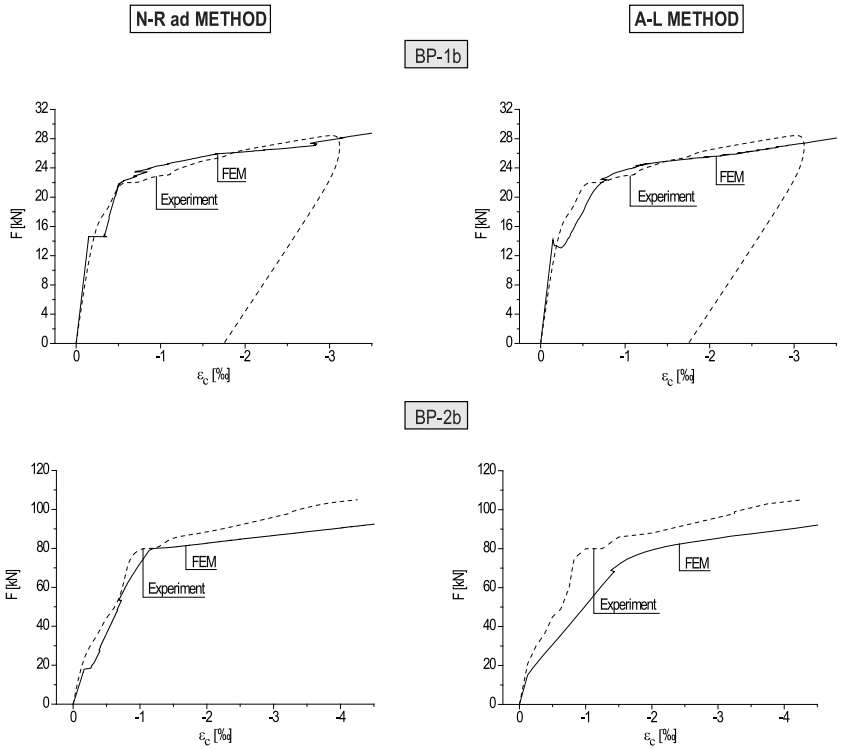

Fig. 5. Comparison of strains in outer layer of concrete in mid span of BP beams

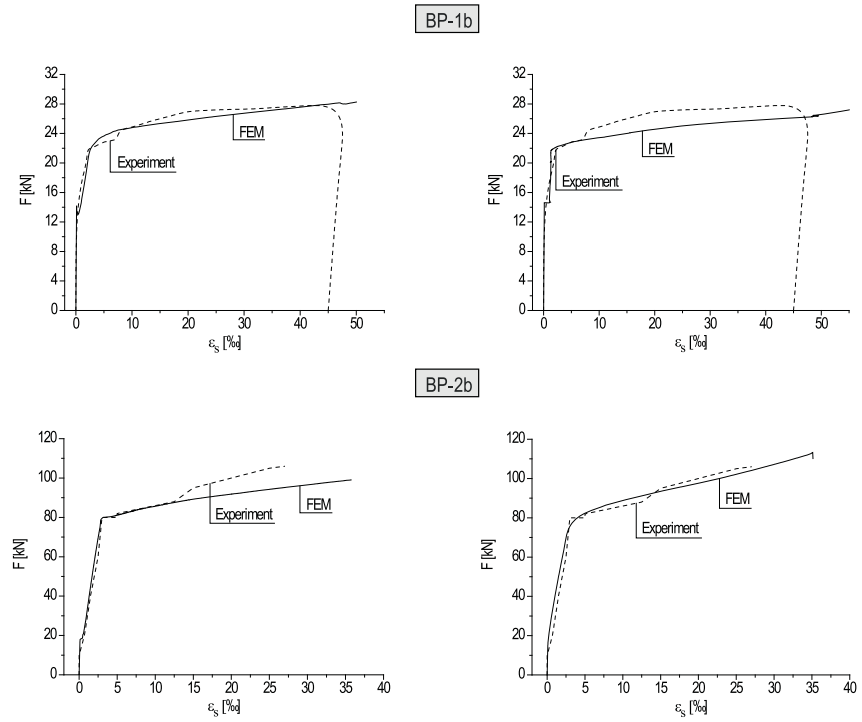

Fig. 6. Comparison of strains in in longitudinal bar in mid span of BP beams

The registration of strain changes in tensile reinforcement bar depending on the load level is performed in the mid span cross-section of the beams, Figure 6.

In case of the experimental curve BP-1b also shows the unloading branch member. The numerical results are almost identical in the linear-elastic range as the experimental data.

Load capacity and displacement analysis

Nonlinear load-displacement in the mid span of beams received in numerical analysis in comparison with experimental results are shown in the Figure 7.

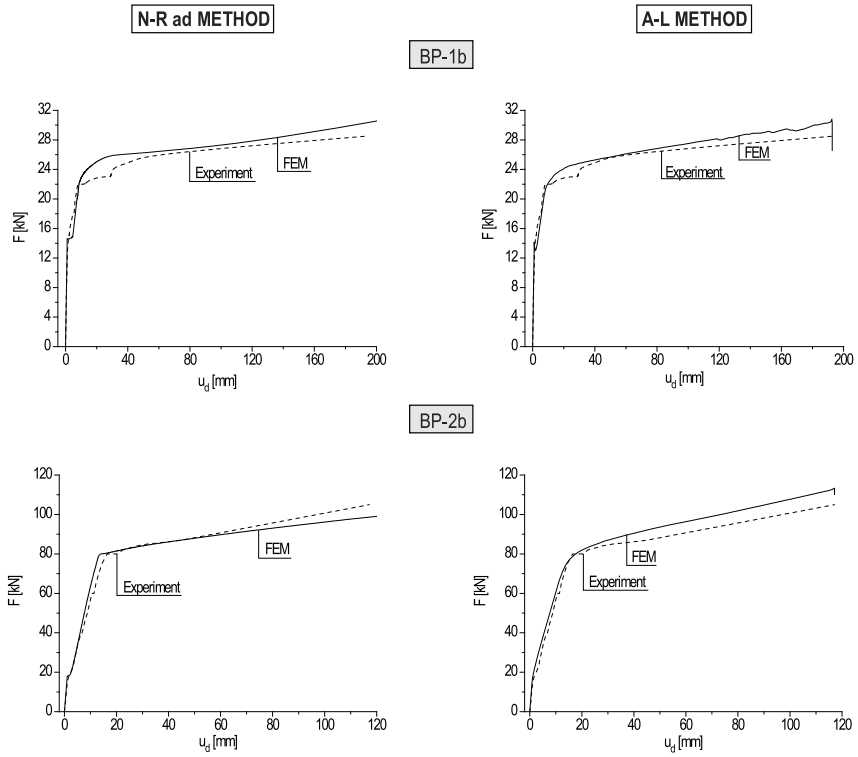

Fig. 7. Comparison of load-displacement at mid span of BP beams

The incremental-iterative methods, both the adaptive descent and the arc-length, give satisfactory numerical results, qualitatively consistent with the experiments. The study on reinforced concrete beams by *e.g.* (Fabbrocino, Pecce 1999, Ashour 2000, Rashid, Mansur 2005), using precise measuring apparatus show that the effects of cracks in the tension zone are not entirely compensated by the elastic properties of steel and plastic properties in the concrete compression zone. Therefore, softening effects are observed on the curve load-displacement as a sudden load capacity drop. These results in presented numerical calculations are possible to obtained using arc-length calculation algorithm which allows to generate a complete load-displacement path with local and global stiffness softening of the structure. In addition, the arc-length method is characterized by high efficiency, because a variable increment step load and properly selected the arc-length parameters provides significant reduction in computation time and makes it possible to obtain very precise numerical solution.

Conclusions

In the modeling of reinforced concrete as simple as possible the finite elements should be used in order to obtain an accurate solution in accepted time. Moreover, especially important is modeling of steel plates in areas of support and load application reflecting the real boundary conditions.

The use of the incremental-iterative arc-length method allows to obtain a complete path of load-deflection with both local and global softening. Moreover, the method is characterized by high efficiency; a variable step of load increments and properly selected arc-length parameters guarantee shortening the time of numerical computing, and additionally very precise solutions. In the presented paper the usefulness of the arc-length method was verified on a spatial numerical model of the reinforced concrete beams with consideration of the concrete softening during compression and tension. The numerical solutions obtained for the reinforced concrete beams are coherent with the experimentally obtained results. This fact indicates the correctness of concrete and reinforcement steel constitutive models and detailed parameters determined these models.

References:

1. Aïtcin P.C. (1998), *High-Performance Concrete*. E & FN SPON.
2. Ashour S.A. (2000), *Effect of Compressive Strength and Tensile Reinforcement Ratio on Flexural Behaviour of High-Strength Concrete Beams*. Engineering Structures, Vol. 22, No 5, 413-423.
3. Bernardi S., Mesureur B., and Rivvilon P.H. (1999), *Cracking of Reinforced High-Strength Concrete Structures.* Proc. 5th International Symposium on Utilization of High Strength / High Performance Concrete, Sandefjord, Norway, Vol. I, 147-153.
4. Calderone M.A. (2009), *High-Strength Concrete. A practical guide.* Taylor & Francis.
5. Comité Euro-Internacional du Beton (1995), *High Performance Concrete. Recommended to the Model Code 90. Research Need.* Bulletin d'Information, Nr 228.
6. Crisfield M.A. (1983). "An arc-length method including line searches and accelerations." *International Journal for Numerical Methods in Engineering*, 19, 1269-1289.
7. Eggert G.M., Dawson P.R., and Mathur K.K. (1991), *An Adaptive Descent Method for Nonlinear Viscoplasticity*. International Journal for Numerical Methods in Engineering, Vol. 31, 1031-1054.
8. Fabbrocino G., Pecce M. (1999), *Experimental Analysis of Influence of Flexure-Shear Interaction on the Rotation Capacity of HPC Beams.* Proc. 5th International Symposium on Utilization of High Strength / High Performance Concrete, Sandefjord, Norway, Vol. I, 243-252.
9. Forde B.W.R., Stiemer S.F. (1987), *Improved arc length orthogonality methods for nonlinear finite element analysis.* Computers and Structures, 27, 625-630.
10. Kamińska M.E. (1999), *Experimental research on HSC one-dimensional members.* Department of Concrete Structures Technical University of Łódź, Poland.

11. Kamińska M.E. (2002), *High-strength Concrete and steel interaction in RC members.* Cement and Concrete Composites, 24, 281-295.
12. Klisiński M. (1984), *Degradation and plastic deformation of concrete*. Institute of Fundamental Technological Research Polish Academy of Sciences Report, Warsaw, Poland, 38, (in Polish).
13. Lambotte H., Taerwe L.R. (1990), *Deflection and Cracking of High Strength Concrete Beams and Slabs.* High-Strength Concrete, Second International Symposium, SP-121, W.T. Hester, ed., American Concrete Institute, Farmington Hills, Michigan, 109-128.
14. Ottosen N.S. (1977), *A failure criterion for concrete.* Journal of the Engineering Mechanics Division, American Society of Civil Engineering, 103, EM 4, 527-535.
15. Pecce M., Fabbrocino G. (1999), *Plastic Rotation Capacity of Beams in Normal and High-Performance Concrete*. ACI Structural Journal, 290-296.
16. Rashid M.A., Mansur M.A. (2005), *Reinforced High-Strength Concrete Beams in Flexure*. ACI Structural Journal, Vol. 102, Nr 3, 462-471.
17. Smarzewski P. (2011), Modelling of static behaviour of inelastic reinforced high-strength concrete beams. *Monographs – Lublin University of Technology*, Lublin, Poland, (in Polish).
18. Stolarski A. (2004), *Dynamic Strength Criterion for Concrete.* Journal of Engineering Mechanics, *ASCE*, Vol. 130, Nr 12, 1428-1435.
19. Taerwe L.R. (1991), *Brittleness versus Ductility of High Strength Concrete.* Structural Engineering Journal, 4, 40-45.
20. Willam K.J., and Warnke E.P. (1975), *Constitutive Model for the Triaxial Behavior of Concrete*. Proceedings, International Association for Bridge and Structural Engineering, Vol. 19, ISMES, Bergamo, Italy.